JOINT EUROPEAN TORUS

JET–P(91)47

J. O'Rourke, F. Rimini, D.F.H. Start
and JET Team

Perturbative Measurements of the Electron Transport Matrix using ICRF Power Modulation

Perturbative Measurements of the Electron Transport Matrix using ICRF Power Modulation

J. O'Rourke, F. Rimini, D.F.H. Start
and JET Team*

JET-Joint Undertaking, Culham Science Centre, OX14 3DB, Abingdon, UK

** See Appendix 1*

Preprint of Paper to be submitted for publication in
Nuclear Fusion (Letters)

ABSTRACT.
Perturbations of the electronic temperature and density produced by Ion Cyclotron Resonance Frequency (ICRF) power modulation in JET are analyzed in terms of coupled transport equations. The incremental heat diffusivity is an order of magnitude larger than the incremental particle diffusivity. Off-diagonal transport plays a significant role by coupling the temperature perturbations into the particle balance equation. These results are in close agreement with recent analyses of heat and density pulse propagation following a sawtooth collapse.

1. INTRODUCTION

The determination of transport coefficients from the evolution of transient perturbations is an area of active research in Tokamak physics /1/ One technique which is frequently employed makes use of the perturbations generated by sawtooth instabilities ("sawtooth pulse propagation") /2,3,4,5,6/. A number of important results have been obtained in JET by this technique /3,5/ , among these:

1. The heat diffusivity inferred from heat pulse analysis χ_e^{hp}, exceeds the heat diffusivity derived from power balance analysis, χ_e^{pb} by a factor of 2 to 5,

2. χ_e^{hp} exceeds the particle diffusivity inferred from density pulse analysis, $D_p^{\Phi p}$, by a factor close to 10,

3. Temperature perturbations generate density perturbations.

The first of these demonstrates that the heat flux is not proportional to the temperature gradient, implying the existence of a "heat pinch" /7,8/ or a "critical temperature gradient" /9/. The second result suggests that electrostatic turbulence (which leads to $\chi_e/D_p \sim 1 - 3$) is not the dominant mechanism in thermal transport /10/. The third result implies the existence of finite off-diagonal terms in the electron transport matrix /5,6/.

It has been suggested recently that effects proper to the sawtooth instability can give rise to an "extended perturbation", vitiating inferences about the underlying transport /11/. Although the analysis in /11/ has been disputed /12/, it is nevertheless important to demonstrate that the above results are not dependent on the particular perturbative technique employed and are therefore not an artifact of the sawtooth instability.

The results pertaining to the ratios χ_e^{hp}/χ_e^{pb} and χ_e^{hp}/D_p^e have been confirmed by ICRF power modulation experiments /13/ and diagnostic pellet injection /10/. In this paper we address the existence of off-diagonal terms in the electron transport matrix. We show that ICRF modulation experiments confirm the results of sawtooth pulse propagation analysis.

In section 2 we describe the ICRF modulation experiments and the analysis procedure used to determine an electron transport matrix. In section 3 we present the results. We summarize our results in section 4.

2. EXPERIMENT AND ANALYSIS TECHNIQUE

Figure 1 shows an overview of pulse 14613. This is a 2MA, 3.4T, $D(He^3)$ discharge bounded by a material (C) limiter, in which a 1.5 sec. period of sawtooth suppression ("Monster sawtooth") is created by the application of ICRF power (32 MHz) with the minority resonance near the magnetic axis. This allows transport to be studied without the complication of periodic redistributions of the temperature and density profiles due to sawteeth /14/. The ICRF power is modulated with an approximately square wave form between 6 and 9 MW, at 4 Hz.

The electron temperature modulations are studied using a 12-channel ECE polychromator /15/. The electron density modulations are studied using a 6-channel far-infrared interferometer /16/. The electron temperature and density are Fourier analyzed to yield the local phase and amplitude of the components It has been verified that the same results are obtained for the density perturbations independently of the order of the Abel and Fourier transformations, as should be the case since these transformations are linear.

The particle and heat balance equations are:

$$\frac{\partial n_e}{\partial t} + \nabla \cdot \Gamma_e = S_e$$

$$\frac{\partial}{\partial t}\left(\frac{3n_eT_e}{2}\right) + \nabla \cdot q_e^{cond} + \nabla \cdot \left(\frac{5}{2} T_e\Gamma_e\right) - \frac{\Gamma_e}{n_e} \cdot \nabla p_e = Q_e$$

where n_e is the electron density, T_e is the electron temperature, $p_e = n_eT_e$ is the electron pressure, Γ_e is the electron particle flux, q_e^{cond} is the (conducted) electron heat flux and S_e and Q_e are the net electron particle and heat sources. These equations are solved numerically for harmonic perturbations of the particle and heat sources, yielding simulations of the phase and amplitude of the temperature and density modulations. We assume that the transport is described by a matrix A defined by

$$-\begin{pmatrix} \tilde{\Gamma}_e/n_e \\ \tilde{q}_e^{cond}/n_eT_e \end{pmatrix} = A\begin{pmatrix} \nabla\tilde{n}_e/n_e \\ \nabla\tilde{T}_e/T_e \end{pmatrix}$$

The elements of A are assumed to be radially constant in order to reduce the number of free parameters to a minimum. Since the transport coefficients are determined only in a limited spatial range ($0 < r/a < 0.3$), this assumption is reasonable. The diagonal transport coefficients, A_{11} and A_{22} correspond to the incremental particle and heat diffusivities, D_e^{inc} and χ_e^{inc}. The off-diagonal terms are a measure of the coupling between heat and particle transport. The elements of the transport matrix are varied to obtain a fit to the data.

The ICRF power deposition is modelled as follows: The coupled power at the modulation frequency is obtained by Fourier analysis of the total coupled power. 80% of the coupled power (this is determined from the modulation of the total plasma energy) contributes to central heating. The electron heating consists of direct heating and indirect heating by collisions with minority ions. Both of these

components are assumed to have a gaussian profile with width W_p. W_p is, in principle, a free parameter along with the matrix elements of A. Previous studies have shown $W_p \sim 0.18m.$, in reasonable agreement with global wave and Fokker-Planck calculations /13/, and this value is used here. The direct heating power density is obtained from $\partial T_e/\partial t$ at the RF switch-on and switch-off times, yielding a direct power fraction of 0.075. The remaining (indirect) power is reduced by a factor $1/(1 - i\omega\tau_S)$ to account for the slowing down time of the minority ions (τ_S is the classical (Spitzer) slowing down time. calculated in this case to be 0.16 sec.).

The modulated electron source is assumed to be localized near the plasma boundary, with a gaussian profile of width W_s, which is adjusted to match the observed density modulations in the outer half of the plasma radius. The phase of the modulated electron source is determined by Fourier analysis of the deuterium Balmer- α emission measurements.

3. RESULTS

Figure 2 shows the measured and modelled phase and amplitude of the temperature data. Figure 3 shows the corresponding density data. The temperature phase has a minimum, and the amplitude a maximum near the magnetic axis (3.2 m.). This confirms that the power deposition is peaked on axis. A remarkable feature of the density modulation is that the amplitude also has a maximum on axis. In the absence of coupling one would have to assume that there exists a modulated source of electrons peaked on axis. However, as the simulations demonstrate, this assumption is not necessary if coupling is taken into account.

The calculated $\tilde{T}_e$ takes into account displacements of the plasma column caused by modulation of the Shafranov shift, using the magnetic axis position as determined by pick-up coil measurements and assuming a linear decrease of the modulation amplitude with radius. A close fit to the data is obtained. Note that the asymmetry about the magnetic axis of the T_e amplitude is attributable to these displacements.

In order to simulate the density data as closely as possible, the calculated $\tilde{n}_e(r)$ is integrated along the interferometer lines of sight. The resulting modulated line-integral densities are Abel-inverted and compared with the data. Thus the limited spatial resolution of the interferometric data is incorporated into these simulations.

The transport matrix corresponding to the simulations is:

$$A\,(m^2\,\mathrm{sec}^{-1}) = \begin{pmatrix} 0.3 & -0.6 \\ 0.0 & 2.4 \end{pmatrix} \qquad 0 < r/a < 0.3$$

A direct comparison with the results obtained from the analysis of sawtooth pulse propagation /6/ is not possible since in that case the transport matrix is determined at a different minor radius (typically $r/a \sim 0.7$). Nevertheless, the two methods give very similar results. We find that $\chi_e^{inc} \sim \chi_e^{hp}$, and $\chi_e^{inc} \gg D_e^{inc}$. Regarding the coupling of density and temperature modulations, we find $A_{12} \sim -2A_{11} \sim -0.6 m^2 s^{-1}$, leading to a density modulation associated with the temperature modulation having $(\tilde{n}_e/n_e) \,/\, (T_e/T_e) \sim -0.3$, also in good agreement with the sawtooth pulse observations.

Figure 4 shows the sensitivity of the simulations to the elements of the transport matrix. $A_{22}\,(\chi_e^{inc})$ and A_{12} are determined within about $\pm$ 30%. The data are not very sensitive to $A_{11}\,(D_e^{inc})$, but values larger than $1 m^2\,\mathrm{sec}^{-1}$ can be excluded. Indeed, the data favour $A_{11} < 0.1 m^2 s^{-1}$, in agreement with a recent analysis of both electron and impurity transport which suggests that at small minor radii the particle diffusion coefficients approach their neo-classical values /17/. As in the case of sawtooth pulse propagation, A_{21} can not be determined. In these simulations we have taken $A_{21} = 0$, but the results are not significantly affected if a symmetric transport matrix ($A_{21} = A_{12}$) is assumed.

CONCLUSIONS

Simultaneous measurements of electron density and temperature on JET have allowed the determination of a 2 X 2 transport matrix. This matrix represents the simplest model of coupled transport and the only one accessible experimentally at present. In general, electron transport could be driven by other forces (such as the ion temperature gradient and the parallel electric field) so that the observed coupling could result from perturbations to quantities other than the electron density and temperature.

The existence of a non-zero off-diagonal element, A_{12} in the transport matrix implies that temperature perturbations are not "eigenmodes" . Thus, if a pure temperature perturbation is launched, it does not remain a pure perturbation but generates a density perturbation. This accompanying density perturbation is transported at the same rate as the temperature perturbation. The ICRF modulation experiment reported here shows that electron temperature perturbations generate density perturbations with $(\tilde{n}_e/n_e)/(\tilde{T}_e/T_e) \sim -0.3$, corresponding to $A_{12} \sim -0.6 m^2 s^{-1}$.

The effect of off-diagonal transport coefficients on the the determination of the diagonal coefficients is small and gives rise to corrections which lie within the error bars of the measurements. This is so because $A_{22} \gg A_{11}$, leading to eigenmodes whose time-scales are well separated.

As noted in the introduction, the total particle and heat fluxes can not be determined from the transport matrix, A, which relates incremental changes in these fluxes to incremental changes in the density and temperature gradients.

ACKNOWLEDGEMENTS

The authors are indebted to their colleagues at JET, especially those responsible for diagnostic and ICRF plant operation.

REFERENCES

/1/ Lopes Cardozo N.J., de Haas J.C.M., Hogeweij G.M.D., et al.. Plasma Physics and Controlled Fusion 32(1990)983.

/2/ Fredrickson E.D., Callen J.D. McGuire K., et al. Nuclear Fusion 26(1986)849.

/3/ Tubbing B.J.D., Lopes-Cardozo N.J., and van der Wiel M.J.. Nuclear Fusion 27, p1843.

/4/ Kim S.K., Brower D.L., Peebles W.A., et al.. Phys Rev. Lett. 60(1988)577.

/5/ de Haas J.C.M., O'Rourke J., Sips A.C.C., et al.. Nuclear Fusion 31(1991)1261.

/6/ Hogeweij G.M.D., O'Rourke J. and Sips A.C.C.. Plasma Physics and Controlled Fusion 33(1991)189.

/7/ Callen J.D., et al. Nuclear Fusion 27(1987)1857

/8/ O'Rourke, J.. Nuclear Fusion 27(1987)2075

/9/ Rebut P.-H., Lallia P., and Watkins M.L.. Plasma Physics and Controlled Nuclear Fusion Research (Proc. 12th. Int. Conf., Nice, 1988), Vol II, IAEA, Vienna (1989)191.

/10/ Gondhalekar A., Cheetham A.D., de Haas J.C.M., et al.. Plasma Physics and Controlled Fusion 31(1989)805

/11/ Fredrickson E.D., et al.. Phys. Rev. Lett. 65(1990)2869

/12/ Lopes-Cardozo N.J. and Sips A.C.C.. Submited for publication in Nuclear Fusion.

/13/ Start D.F.H., Bhatnagar V.P., Boyd D.A., et al.. Nucl. Fusion Suppl. 29(1989)593.

/14/ Gambier D.J., Evrard M.P., Adam J., et al.. Nuclear Fusion 30(1990)23

/15/ Tubbing B.J.D., Barbian E., Campbell D.J., et al.. Proc. 12th European Conference on Controlled Fusion and Plasma Physics, Budapest, 215.

/16/ Braithwaite G., Gottardi N., Magyar G., et al.. Rev. Sci. Inst. 60(1989)2825

/17/ Giannella R., Hawkes N.C., Lauro Taroni L., et al.. 18th European Conference on Controlled Fusion and Plasma Physics, Berlin. JET-P(91)08.

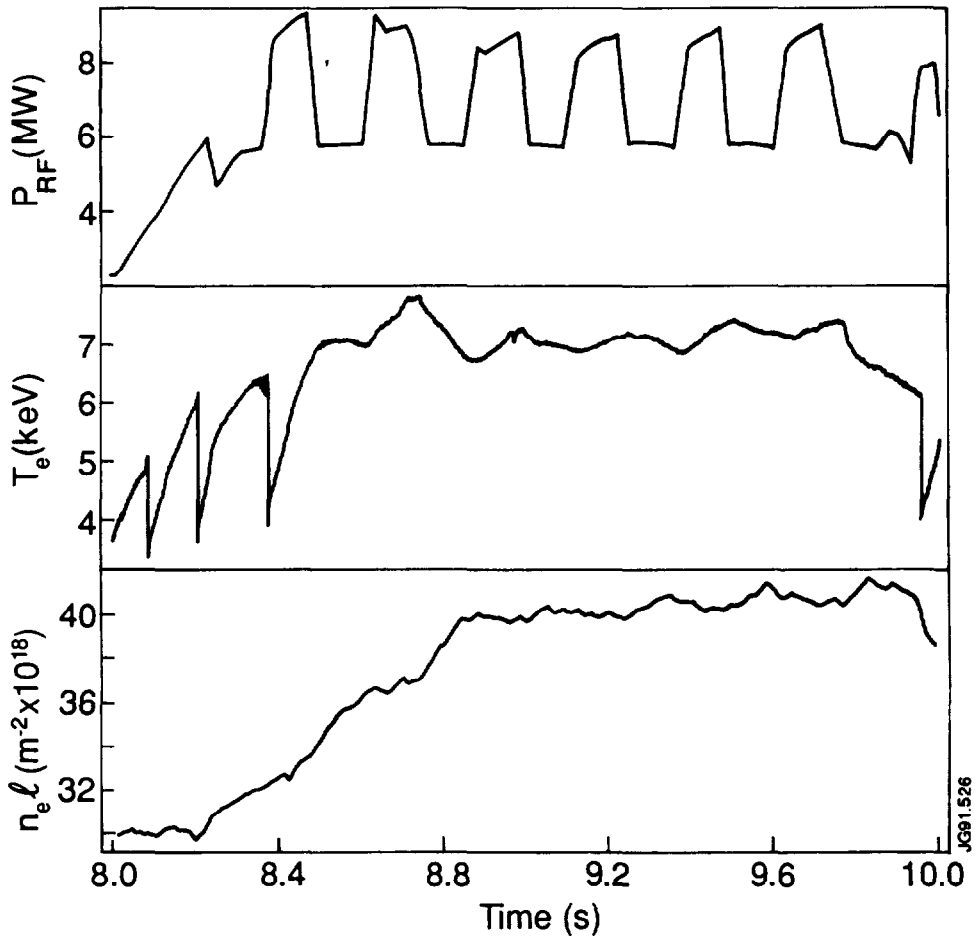

Fig. 1 - Time evolution of the coupled ICRF power, the electron temperature (at R = 3.15 m.) and the Abel-inverted electron density (at R = 3.15 m.) in pulse 14613. The Fourier analysis is performed in the interval 48.8 to 49.8 s..

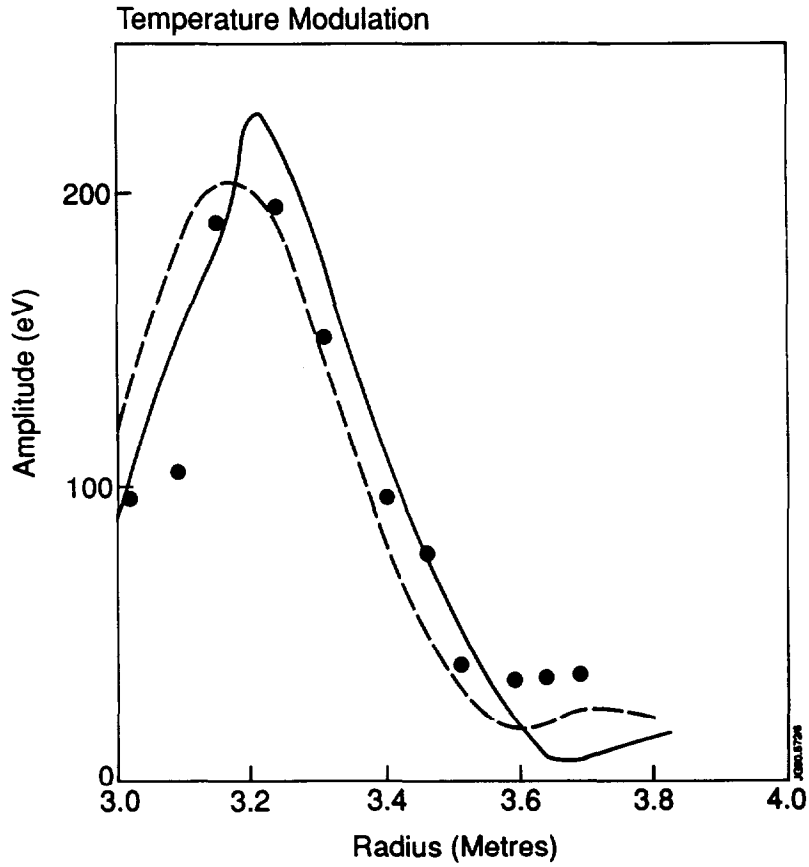

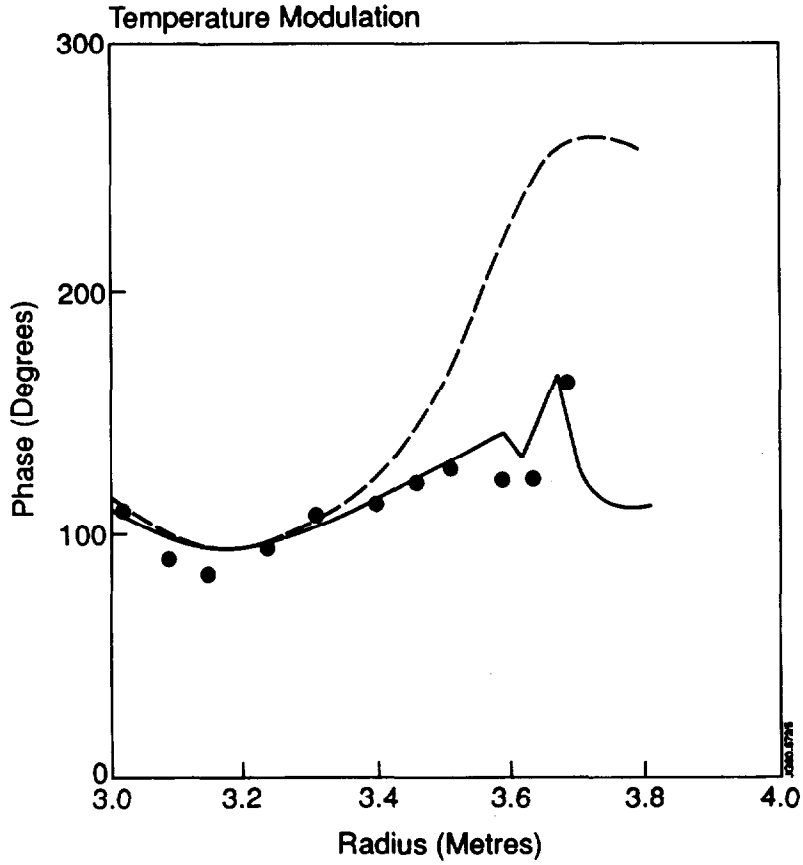

Fig. 2 - Temperature phase (a) and amplitude (b) in pulse 14613. Circles -- data, dashed line -- simulation without Shafranov shift modulation, solid line -- simulation with Shafranov shift modulation.

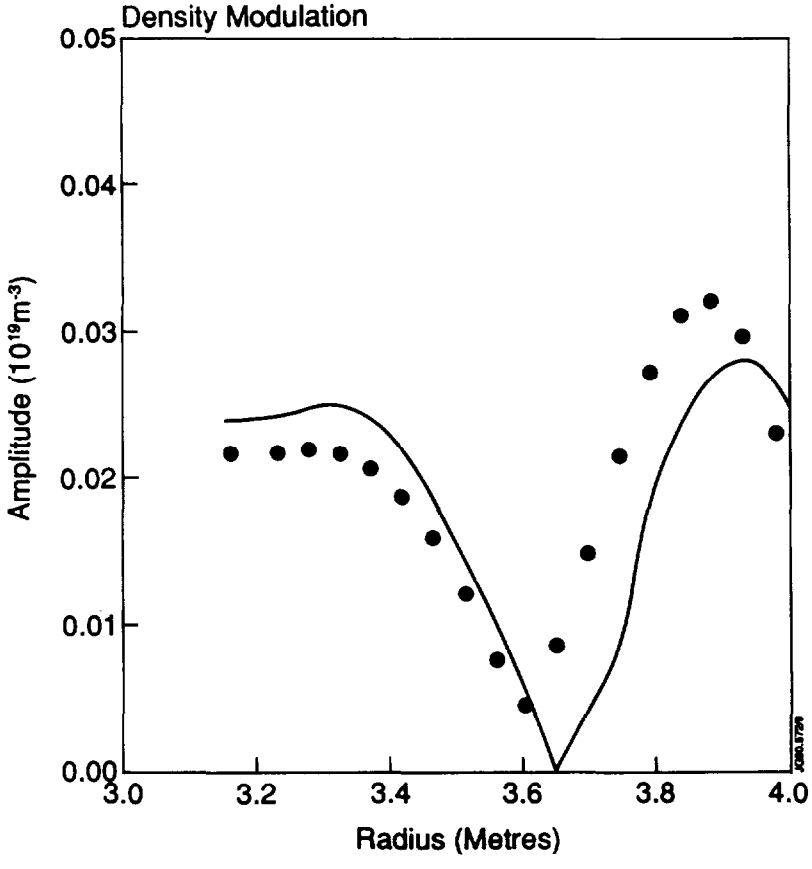

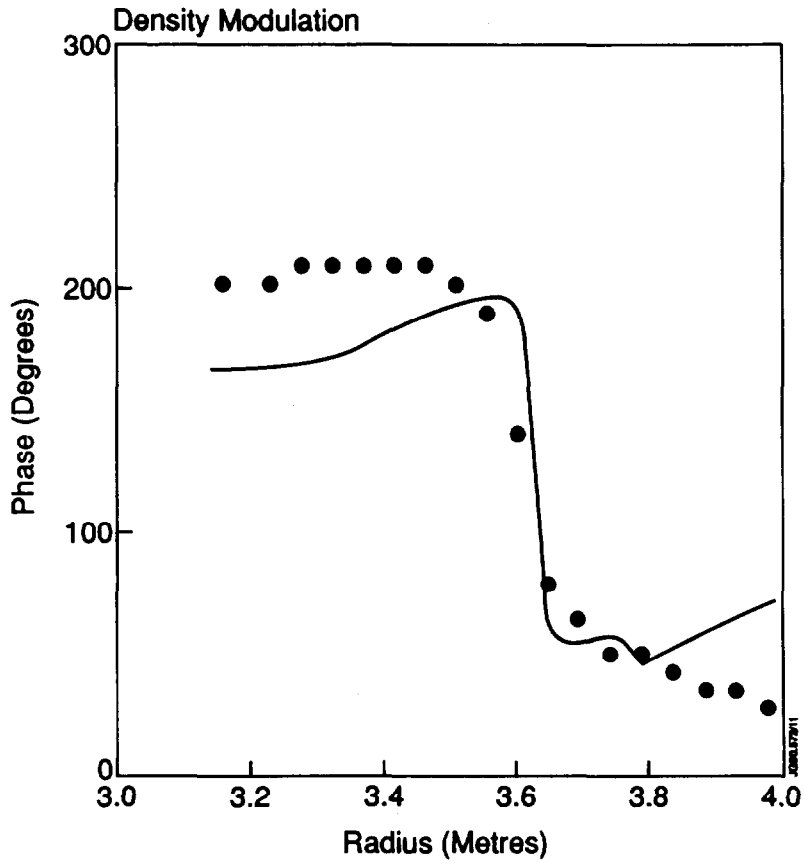

Fig. 3 - Density phase (a) and amplitude (b) in pulse 14613. Circles -- data, solid line -- simulation.

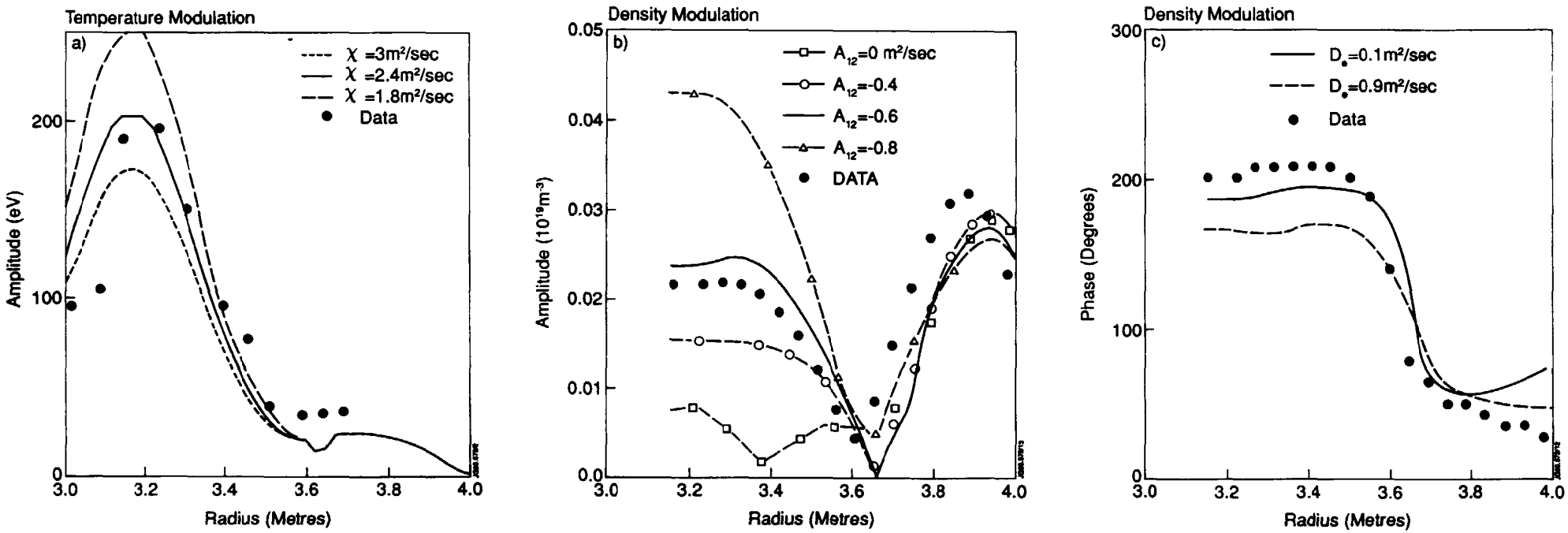

Fig. 4 - Sensitivity of the simulations in Fig. 2)and 3) to variations of A_{22} (a), A_{12} (b) and A_{11} (c).

Appendix I

THE JET TEAM

JET Joint Undertaking, Abingdon, Oxon, OX14 3EA, U.K.

J.M. Adams[1], H. Altmann, A. Andersen[14], P. Andrew[18], M. Angelone[29], S.A. Arshad, W. Bailey, P. Ballantyne, B. Balet, P. Barabaschi, R. Barnsley[2], M. Baronian, D.V. Bartlett, A.C. Bell, I. Benfatto[5], G. Benali, H. Bergsaker[11], P. Bertoldi, E. Bertolini, V. Bhatnagar, A.J. Bickley, H. Bindslev[14], T. Bonicelli, S.J. Booth, G. Bosia, M. Botman, D. Boucher, P. Boucquey, P. Breger, H. Brelen, H. Brinkschulte, T. Brown, M. Brusati, T. Budd, M. Bures, T. Businaro, P. Butcher, H. Buttgereit, C. Caldwell-Nichols, D.J. Campbell, P. Card, G. Celentano, C.D. Challis, A.V.Chankin[23], D. Chiron, J. Christiansen, C. Christodoulopoulos, P. Chuilon, R. Claesen, S. Clement, E. Clipsham, J.P. Coad, M. Comiskey[4], S. Conroy, M. Cooke, S. Cooper, J.G. Cordey, W. Core, G. Corrigan, S. Corti, A.E. Costley, G. Cottrell, M. Cox[7], P. Cripwell, H. de Blank[15], H. de Esch, L. de Kock, E. Deksnis, G.B. Denne-Hinnov, G. Deschamps, K.J. Dietz, S.L. Dmitrenko, J. Dobbing, N. Dolgetta, S.E. Dorling, P.G. Doyle, D.F. Düchs, H. Duquenoy, A. Edwards, J. Ehrenberg, A. Ekedahl, T. Elevant[11], S.K. Erents[7], L.G. Eriksson, H. Fajemirokun[12], H. Falter, D. Flory, J. Freiling[15], C. Froger, P. Froissard, K. Fullard, M. Gadeberg, A. Galetsas, D. Gambier, M. Garribba, P. Gaze, R. Giannella, A. Gibson, R.D. Gill, A. Girard, A. Gondhalekar, C. Gormezano, N.A. Gottardi, C. Gowers, B.J. Green, R. Haange, G Haas, A. Haigh, G. Hammett[6], C.J. Hancock, P.J. Harbour, N.C. Hawkes[7], P. Haynes[7], J.L. Hemmerich, T. Hender[7], F.B. Herzog, R.F. Herzog, J. Hoekzema, J. How, M. Huart, L Hughes, T.P. Hughes[4], M. Hugon, M. Huguet, A. Hwang[7], B. Ingram, M. Irving, J. Jacquinot, H. Jaeckel, J.F. Jaeger, G. Janeschitz[13], S. Jankowicz[22], O.N. Jarvis, F. Jensen, E.M. Jones, L.P.D.F. Jones, T.T.C. Jones, J-F. Junger, E. Junique, A. Kaye, B.E. Keen, M. Keilhacker, G.J. Kelly, W. Kerner, R. Konig, A. Konstantellos, M. Kovanen[20], G. Kramer[15], P. Kupschus, R. Lässer, J.R. Last, B. Laundy, L. Lauro-Taroni, K. Lawson[7], M. Lennholm, A. Loarte, R. Lobel, P. Lomas, M. Loughlin, C. Lowry, B. Macklin, G. Maddison[7], G. Magyar, W. Mandl[13], V. Marchese, F. Marcus, J. Mart, E. Martin, R. Martin-Solis[8], P. Massmann, G. McCracken[7], P. Meriguet, P. Miele, S.F. Mills, P. Millward, R. Mohanti[17], P.L. Mondino, A. Montvai[3], S. Moriyama[28], P. Morgan, H. Morsi, G. Murphy, M. Mynarends, R. Myrnäs[16], C. Nardone, F. Nave[21], G. Newbert, M. Newman, P. Nielsen, P. Noll, W. Obert, D. O'Brien, J. O'Rourke, R. Ostrom, M. Ottaviani, M. Pain, F. Paoletti, S. Papastergiou, D. Pasini, A. Peacock, N. Peacock[7], D. Pearson[12], R. Pepe de Silva, G. Perinic, C. Perry, M. Pick, R. Pitts[7], J. Plancoulaine, J-P. Poffé, F. Porcelli, L. Porte[19], R. Prentice, S. Puppin, S. Putvinsko[23], G. Radford[9], T. Raimondi, M.C. Ramos de Andrade, P-H. Rebut, R. Reichle, E. Righi, F. Rimini, D. Robinson[7], A. Rolfe, R.T. Ross, L. Rossi, R. Russ, P. Rutter, H.C. Sack, G. Sadler, G. Saibene, J.L. Salanave, G. Sanazzaro, A. Santagiustina, R. Sartori, C. Sborchia, P. Schild, M. Schmid, G. Schmidt[6], B. Schunke, S.M. Scott, A. Sibley, R. Simonini, A.C.C. Sips, P. Smeulders, R. Stankiewicz[27], M. Stamp, P. Stangeby[18], D.F. Start, C.A. Steed, D. Stork, P.E. Stott, T.E. Stringer, P. Stubberfield, D. Summers, H. Summers[19], L. Svensson, J.A. Tagle[21], A. Tanga, A. Taroni, A. Tesini, P.R. Thomas, E. Thompson, K. Thomsen, J.M. Todd, P. Trevalion, B. Tubbing, F. Tibone, E. Usselmann, H. van der Beken, G. Vlases, M. von Hellermann, T. Wade, C. Walker, R. Walton[6], D. Ward, M.L. Watkins, M.J. Watson, S. Weber[10], J. Wesson, T.J. Wijnands, J. Wilks, D. Wilson, T. Winkel, R. Wolf, B. Wolle[24], D. Wong, C. Woodward, Y. Wu[25], M. Wykes, I.D. Young, L. Zannelli, Y. Zhu[26], W. Zwingmann.

PERMANENT ADDRESSES

1. UKAEA, Harwell, Didcot, Oxon, UK.
2. University of Leicester, Leicester, UK.
3. Central Research Institute for Physics, Academy of Sciences, Budapest, Hungary.
4. University of Essex, Colchester, UK.
5. ENEA-CNR, Padova, Italy.
6. Princeton Plasma Physics Laboratory, New Jersey, USA.
7. UKAEA Culham Laboratory, Abingdon, Oxon, UK.
8. Universidad Complutense de Madrid, Spain.
9. Institute of Mathematics, University of Oxford, UK.
10. Freien Universität, Berlin, F.R.G.
11. Swedish Energy Research Commission, S-10072 Stockholm, Sweden.
12. Imperial College of Science and Technology, University of London, UK.
13. Max Planck Institut für Plasmaphysik, Garching bei München, FRG.
14. Risø National Laboratory, Denmark.
15. FOM Instituut voor Plasmafysica, 3430 Be Nieuwegein, The Netherlands.
16. University of Lund, Sweden.
17. North Carolina State University, Raleigh, NC, USA
18. Institute for Aerospace Studies, University of Toronto, Downsview, Ontario, Canada.
19. University of Strathclyde, 107 Rottenrow, Glasgow, UK.
20. Nuclear Engineering Laboratory, Lapeenranta University, Finland.
21. CIEMAT, Madrid, Spain.
22. Institute for Nuclear Studies, Otwock-Swierk, Poland.
23. Kurchatov Institute of Atomic Energy, Moscow, USSR
24. University of Heidelberg, Heidelberg, FRG.
25. Institute for Mechanics, Academia Sinica, Beijing, P.R. China.
26. Southwestern University of Physics, Leshan, P.R. China.
27. RCC Cyfronet, Otwock Swierk, Poland.
28. JAERI, Naka Fusion Research Establishment, Ibaraki, Japan.
29. ENEA, Frascati, Italy.

At 1st June 1991